Non-Gaussian effects, space-time decoupling, and mobility bifurcation in glassy hard-sphere fluids and suspensions

Erica J. Saltzman and Kenneth S. Schweizer*

Department of Materials Science and Frederick Seitz Materials Research Laboratory, University of Illinois, 1304 West Green Street, Urbana, Illinois 61801, USA

(Received 23 August 2006; revised manuscript received 17 October 2006; published 12 December 2006)

Brownian trajectory simulation methods are employed to fully establish the non-Gaussian fluctuation effects predicted by our nonlinear Langevin equation theory of single particle activated dynamics in glassy hard-sphere fluids. The consequences of stochastic mobility fluctuations associated with the space-time complexities of the transient localization and barrier hopping processes have been determined. The incoherent dynamic structure factor was computed for a range of wave vectors and becomes of an increasingly non-Gaussian form for volume fractions beyond the (naive) ideal mode coupling theory (MCT) transition. The non-Gaussian parameter (NGP) amplitude increases markedly with volume fraction and is well described by a power law in the maximum restoring force of the nonequilibrium free energy profile. The time scale associated with the NGP peak becomes much smaller than the α relaxation time for systems characterized by significant entropic barriers. An alternate non-Gaussian parameter that probes the long time α relaxation process displays a different shape, peak intensity, and time scale of its maximum. However, a strong correspondence between the classic and alternate NGP amplitudes is predicted which suggests a deep connection between the early and final stages of cage escape. Strong space-time decoupling emerges at high volume fractions as indicated by a nondiffusive wave vector dependence of the relaxation time and growth of the translation-relaxation decoupling parameter. Displacement distributions exhibit non-Gaussian behavior at intermediate times, evolving into a strongly bimodal form with slow and fast subpopulations at high volume fractions. Qualitative and semiquantitative comparisons of the theoretical results with colloid experiments, ideal MCT, and multiple simulation studies are presented.

DOI: 10.1103/PhysRevE.74.061501 PACS number(s): 61.20.Gy, 61.20.Ja, 05.40.Ca, 82.70.Kj

I. INTRODUCTION

The glassy dynamics of colloidal suspensions, hard-sphere fluids, and thermal liquids are intensely studied and unsolved problems [1]. The underlying cause of the precipitous increase of relaxation times and viscosity with decreasing temperature or increasing volume fraction remains a source of controversy. The relative importance of thermodynamics and kinetics continues to be debated, and a wide variety of seemingly disparate models have been proposed [1,2]. The mode-coupling theory (MCT) is a microscopic, force-based description of slow dynamics that has made many unique and important predictions [3]. In its "idealized" form (IMCT) it addresses dynamical slowing down and literal arrest due to many particle caging. By empirically adjusting the location of an ideal nonergodicity transition, IMCT predictions achieve quite good agreement with experiments and simulations for many (but not all) properties in the dynamical precursor regime corresponding to the initial changes of relaxation times and the diffusion constant by 2–4 decades [3]. However, the prediction of an ideal kinetic glass transition (simultaneous divergence of the viscosity and all relaxation times) is not seen in experiment. It is generally agreed that IMCT cannot address the deeply supercooled (or overcompressed) fluid regime where experiments [1], theory [2,4,5], and simulations [2,6–8] suggest activated transport over barriers is likely the dominant factor and heterogeneous dynamics becomes prominent. Computer simulations based on Newtonian [6], Brownian [7], and so-called stochastic [7] dynamics, and also megabasin landscape analyses [8], all find activated hopping is important *at or above (below)* the *empirically* deduced MCT critical temperature (volume fraction).

We have recently developed a theory for *single particle* barrier hopping dynamics based on a nonlinear stochastic Langevin equation. The simplest formulation is for hard-sphere fluids or suspensions [9,10], and the ideas have been extended to treat colloidal gelation [11,12], suspensions composed of rigid nonspherical objects [13], deeply supercooled polymer melts in both the bulk [14,15] and multiple anisotropic situations [16], sub-T_g polymer glasses [17], and nonlinear rheology [18–20]. The volume fraction dependence of the *mean* relaxation time, viscosity, diffusion constant, and other properties of hard-sphere fluids have been quasianalytically computed, and many of the no adjustable parameter results are in good agreement with experiments on athermal suspensions [9,10]. This quasianalytic approach involves a type of mean-field treatment. In reality, glassy fluids exhibit significant dynamic heterogeneity and mobility fluctuations [1,21–25] even in the dynamical precursor regime which are not captured by ideal MCT. An important feature underlying these effects is a broad distribution of characteristic relaxation times and rates.

The most obvious source of dynamic fluctuations in our approach is the stochastic nature of the activated barrier hopping process, a full accounting of which requires numerical solution of a stochastic nonlinear Langevin equation and al-

*Electronic address: kschweiz@uiuc.edu

lows the calculation of all single particle time-dependent quantities. Very recently we presented the conceptual and algorithmic elements required to implement this approach [26]. Results for the mean square displacement, characteristic time scales, decoupling of rates and times, and cage scale relaxation were given. In this paper we complete our study by addressing all non-Gaussian phenomena associated with slow single particle dynamics in hard-sphere fluids. The fluctuation effects of primary interest include the classic and alternate non-Gaussian parameters [27], the wave vector dependence of the incoherent dynamic structure factor, length scale dependent decoupling of diffusion and relaxation, bifurcation of particle mobility into slow and fast subpopulations, and the particle displacement required for recovery of Fickian diffusion.

A primary goal of our recent [26] and present work is to establish how much of the rich dynamics of glassy simple fluids can be understood from the elementary process of activated hopping on the particle (cage) length scale. A second goal is to provide insight concerning the seemingly perplexing question of why ideal MCT can describe many aspects of the precursor regime dynamics well (e.g., transport coefficients, mean square displacements, two-step decay of correlators, etc. [3]), but fails to capture strongly non-Gaussian or dynamic heterogeneity aspects. We note the phrase "dynamic heterogeneity" usually refers to phenomena associated with spatial correlations of the motion of *different* particles as encoded in multipoint (typically four) correlation functions or susceptibilities. The latter are not described by our approach, and hence the present work can be viewed as quantifying the manifestations or implications of dynamic heterogeneity at the standard (and easily measurable) two-point correlation function level.

In Sec. II we briefly review our theory but refrain from repeating the detailed discussions of previous papers, especially the technical aspects of the recent stochastic trajectory-based study [26]. Section III presents calculations of the incoherent dynamic structure factor, its characteristic decay time and degree of nonexponentiality, and wave vector dependent decoupling of diffusion and relaxation. Section IV studies the classic and alternate [27] non-Gaussian parameter. In Sec. V results for the distribution of particle displacements are given, and we conclude in Sec. VI. Throughout the paper our theoretical results are compared to experiments on (nearly) hard core colloidal suspensions and a variety of computer simulations. The comparisons are made at a qualitative and semiquantitative level, a restriction which is unavoidable for two reasons. First, we aim at a no adjustable parameter confrontation with experiment and simulation, not one based on fitting parameters. Second, the experimental suspensions involve slightly charged polydisperse colloids and hydrodynamic effects, and the simulation models are characterized by polydispersity, nonhard core repulsions, and/or involve thermal binary Lennard-Jones mixtures (BLJM), complications beyond the monodisperse hard-sphere fluid model of present study.

II. ENTROPIC BARRIER HOPPING THEORY OF GLASSY DYNAMICS

Our theory of glassy dynamics in hard-sphere fluids was originally heuristically proposed [9] as an extension of naive ideal MCT [28] to treat barrier hopping. Recently a microscopic statistical mechanical derivation has been achieved [29]. The physical motivations, technical approximations and limitations, and numerical implementation are all described in detail elsewhere [9,10,26,29]. Briefly, the approach is built on a locally solid state, or inhomogeneous fluid, picture of slow single particle dynamics as embodied in a stochastic nonlinear Langevin equation in the overdamped (no inertial effects) Brownian regime. For suspensions, hydrodynamic interactions enter only as they influence the short time/distance dissipative dynamics at the one and two particle level. The interparticle force contribution to the stochastic equation of motion is rendered tractable based on a local equilibrium idea common to dynamic density functional theory approaches [30,31]. This allows the instantaneous intermolecular forces that are the origin of caging to be renormalized in an effective potential manner via the structure factor of the fluid [32]. Temporal deviations from locally stable initial positions are modeled in an Einstein solid spirit [28] with particle-displacement dependent Debye-Waller factors [9,29]. Dynamic closure at the tagged particle level is achieved based on a self-consistent approximation [9,28,32] that relates collective local dynamics to its single particle analog.

The closed nonlinear stochastic Langevin equation of motion for the instantaneous scalar particle *displacement* in the overdamped limit is [9,29]

$$\zeta_s \frac{\partial r(t)}{\partial t} = -\frac{\partial F_{eff}[r(t)]}{\partial r(t)} + \delta f(t), \tag{1}$$

where $r(0)=0$, the random force satisfies $\langle \delta f(0)\delta f(t)\rangle = 2k_B T\zeta_s \delta(t)$, and $\zeta_s = k_B T/D_s$ is the short time friction constant (computed based on independent binary collisions [9,10]). The nonequilibrium free energy is

$$F_{eff}(r) = -3\ln(r) - \int \frac{d\vec{q}}{(2\pi)^3}\rho C^2(q)S(q)[1+S(q)]^{-1} \times e^{-(q^2r^2/6)[1+S^{-1}(q)]} \equiv F_{ideal} + F_{excess}, \tag{2}$$

where $C(q)$ and $S(q)$ are the Fourier-transformed direct correlation function and static structure factor, respectively, which are computed based on the Percus-Yevick integral equation theory [32], and ρ is the number density. Results for the nonequilibrium free energy of a hard-sphere fluid (particle diameter σ) and volume fraction ϕ are shown in Fig. 1. A local minimum emerges at $\phi_{MCT}=0.432$ that defines the naive IMCT nonergodicity transition. In our approach this signals the onset of transient particle localization and a crossover to activated dynamics. In the absence of inertial effects the theory applies to both hard-sphere fluids and Brownian colloidal suspensions, differing only in the elementary time scale set by the short time dynamics.

The nonequilibrium free energy (Fig. 1) is a monotonically decreasing function of particle displacement at volume fractions below ϕ_{MCT}. Above the crossover an entropic barrier of height F_B emerges which is proportional (for $\phi \geq 0.5$) to the inverse of the dimensionless isothermal compressibility (inset of Fig. 1). Figure 2 presents important

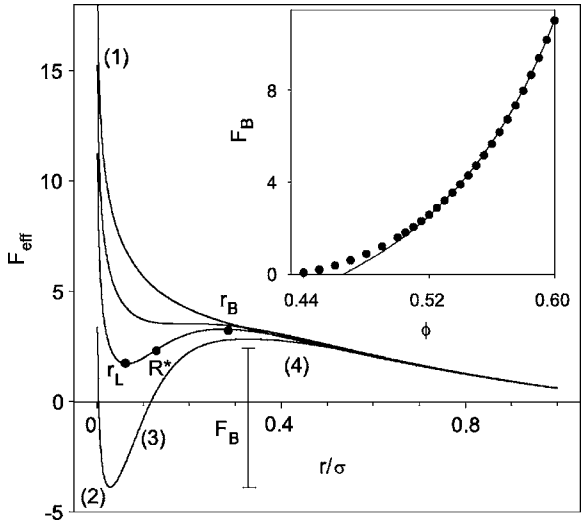

FIG. 1. Nonequilibrium "free energy" (units of thermal energy) as a function of dimensionless displacement for (from top to bottom): ϕ=0.3, 0.432, 0.50, and 0.57. The barrier height is indicated, along with the locations of the local minimum (r_L), barrier (r_B), and maximum restoring force R^* for ϕ=0.5. The four regimes of dynamical behavior (1)-(4) discussed in Ref. [9] are also indicated. Inset: Entropic barrier as a function of volume fraction (points). The smooth curve is a fit to an inverse dependence on the dimensionless compressibility, $F_B \sim 0.08/S_0$, where $S(q=0)=S_0$ [9].

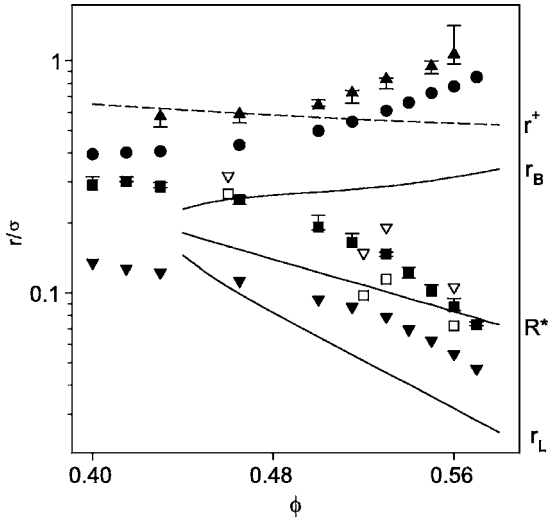

FIG. 2. Length scales. Nonequilibrium free energy profile: localization length (r_L)—lower solid line; location of maximum restoring force R^*—middle solid line; barrier location (r_B)—upper solid line; reaction point ($r^\dagger$)—dashed line. Dynamic length scales determined from numerical solution of the Langevin equation: dynamic localization length defined as the displacement of maximum non-Fickian behavior of $\langle r^2\rangle^{1/2}$ (or the quasiplateau $\langle r^2\rangle^{1/2}_{\text{plateau}}$ [26])—solid down triangles; root mean square displacement (MSD) corresponding to the maximum of classic non-Gaussian parameter (r_α)—solid squares; root MSD corresponding to the maximum of alternate NGP (r_γ)—up triangles; root MSD at the α relaxation time (r_*)—circles. Experimental length scales [45]: root MSD of the maximum non-Fickian behavior of $\langle r^2\rangle^{1/2}$—open down triangles; root MSD corresponding to the maximum of the NGP—open squares.

length scales which include the MCT localization length r_L [displacement corresponding to the minimum of $F_{\text{eff}}(r)$], displacement of the maximum restoring force R^*, and the barrier location, r_B. All length scales are normalized by the hard sphere diameter and energies by k_BT. The mean first passage time over the barrier, τ_K, can be calculated from the high friction version of Kramers theory [33]

$$\frac{\tau_K}{\tau_0} = 2\pi \frac{\zeta_s}{\zeta_0} \frac{e^{F_B/k_BT}}{\sqrt{\tilde{K}_0 \tilde{K}_B}}, \tag{3}$$

where the elementary Brownian time $\tau_0=\sigma^2\zeta_0/k_BT$, for colloids ζ_0 is the Stokes-Einstein friction constant, and $\tilde{K}_0$ and $\tilde{K}_B$ are the dimensionless harmonic curvatures of the well and barrier, respectively [9]. All time scales are expressed in units of the elementary Brownian time.

The dynamics described by Eqs. (1) and (2) places no restrictions on the lifetime of the barrier and allows trajectory recrossing to indefinitely long times. The latter is not physically appropriate since our approach invokes a direct connection between single particle and collective dynamics and barrier hopping signals structural relaxation and the release of caging constraints [26,29]. Hence a dynamical crossover from the local equilibrium picture of Eqs. (1) and (2) to a homogeneous fluid linear three-dimensional (3D) Langevin description is required which is implemented by modifying Eq. (1) as [26]

$$-\frac{\partial F_{eff}}{\partial r(t)} \rightarrow -\zeta_{hop}(\phi)\frac{\partial \vec{r}}{\partial t}. \tag{4}$$

Here a hopping friction constant is introduced to account for the frictional resistance associated with the barrier hopping event. As described previously [26], to quantitatively implement this idea a cage escape displacement or "reaction point" is introduced in analogy with the dividing surface that defines reactants and products in chemical reactions [34]. The reaction point is *not* treated as an adjustable or fitting parameter. Rather, it is computed based on a physically motivated criterion for the validity of the highly-localized form of the translational entropy free energy [35] or irrelevance of the localizing cage force [26]. Alternative implementations of the reaction point idea all yield very similar results corresponding to a weakly volume fraction dependent $r^\dagger \simeq 0.5-0.6$ [26]. The transition in dynamical description from Eqs. (1) and (2) to Fickian motion is executed on a single-trajectory basis. Trajectories that have passed the reaction point diffuse with an enhanced friction constant $\zeta_s \rightarrow \zeta_s + \zeta_{hop}$, where

$$\frac{1}{\zeta_{hop}} = \frac{1}{N}\sum_i \frac{1}{\zeta_{hop,i}}. \tag{5}$$

In Eq. (5) the trajectory friction constant $\zeta_{hop,i} \approx 6t_i^\dagger/r^{\dagger 2}$, $t_i^\dagger$ is the time for the ith trajectory to pass the reaction point, and the number of trajectories, N, is typically 40 000 [26]. A "hopping diffusion constant" can be defined, $D_{hop}=k_BT/\zeta_{hop}$, and the observable long-time diffusion constant is

$$D = \frac{k_B T}{\zeta_s + \zeta_{hop}}. \quad (6)$$

The above approach invokes the idea that after a reaction event trajectory propagation is described by the standard diffusive Langevin equation with a *unique ensemble averaged* friction constant. We believe this is an internally consistent procedure for switching from a local equilibrium solid-state picture of the fluid to the irreversible viscous limit. The specifics of the method do quantitatively influence our predictions for non-Gaussian fluctuation effects. However, if switching to Cartesian Fickian diffusion is not done then *all* the dynamic fluctuation effects become *larger* than those based on the crossover idea embodied in Eqs. (4)–(6) [26].

A particularly important and relevant prior result is our prediction of the breakdown of the Stokes-Einstein relation between the self-diffusion constant (D) and (α) relaxation time (τ^*, see Sec. III A). At high volume fractions a fractional Stokes-Einstein relation is found, $D \propto (\tau^*)^{-z}$, with $z \sim 0.77$ [26]. Moreover, at $\phi=0.57$ the product or decoupling factor $D\tau^*$ has increased by a factor of ~ 10 relative to its "normal fluid" value ($\phi \sim 0.4$). This is consistent with very recent simulations of a polydisperse hard-sphere-like model which find decoupling factors of $\sim 8-15$ at the highest volume fractions studied [36].

The present work studies the same eleven volume fractions previously examined [26] which fall in the interval $0.4 \leqslant \phi \leqslant 0.57$. The barrier is $\sim 1\ k_B T$ at $\phi=0.5$ and grows to $6.7\ k_B T$.

III. INCOHERENT DYNAMIC STRUCTURE FACTOR

A. Characteristic decay time, superposition, and stretching

The incoherent dynamic structure factor, $F(q,t) \equiv \langle e^{i\vec{q}\cdot\vec{r}(t)} \rangle$, has been computed at five wave vectors: $2.6\ \sigma^{-1}$, a relatively small value; q^*, the first peak of the structure factor; q_2, the second peak of the structure factor; and two wave vectors intermediate between $2.6\ \sigma^{-1}$ and q^*: $q_a(q_b) = 2.6\sigma^{-1} + 1/3(2/3)[q^* - 2.6\sigma^{-1}]$. Results are shown in Fig. 3 for a low ($\phi=0.43$) and high ($\phi=0.55$) volume fraction [37]. For the highest wave vector a clear two-step decay is observed; however, for all smaller wave vectors it is not, perhaps because the theory quantitatively underpredicts the transient localization length and hence the amount of decay of $F(q,t)$ due to the short time dynamical process [26]. For the lower volume fraction [Fig. 3(a)] relaxation clearly slows with decreasing wave vector. However, at high volume fractions the distinction among the various wave vectors becomes less pronounced. For the $\phi=0.55$ case shown, the final decay on all length scales (except $q\sigma=2.6$) is nearly identical. This trend is qualitatively understandable from our prior *general* statistical dynamical analysis as a consequence of non-Fickian motion and a growing viscoelastic correlation length ξ_D [38].

A characteristic wave vector-dependent relaxation time $\tau(q)$ is defined as $F[q, \tau(q)] = 1/e$. The time scale corresponding to relaxation at the first peak of the structure factor, $\tau(q=q^*) = \tau^*$, is a common measure of the structural or α relaxation time. Results are shown in the inset of Fig. 4. The α time increases steeply with volume fraction and is very well described as an exponential function of the barrier height. Ideal MCT [3] inspired critical power law fits, $\tau^* \sim (\phi_c - \phi)^{-\nu}$, with $\phi_c=0.57$ ($\nu=2.4$) and $\phi_c=0.58$ ($\nu=3.0$), also provide a good empirical representation of the relaxation time data except at high volume fractions where such a form cannot described our *non*divergent (below random close packing) theoretical results. The volume fraction dependence of the relaxation times for the other four wave vectors studied are also well fit by critical power laws (not shown). The extracted empirical critical exponents are given in Table I, and modestly increase as the probing length scale diminishes. Despite the length scale variations of apparent exponents, normalization of the $\tau(q)$ calculations for each wave vector by the corresponding $\phi=0.5$ value results in

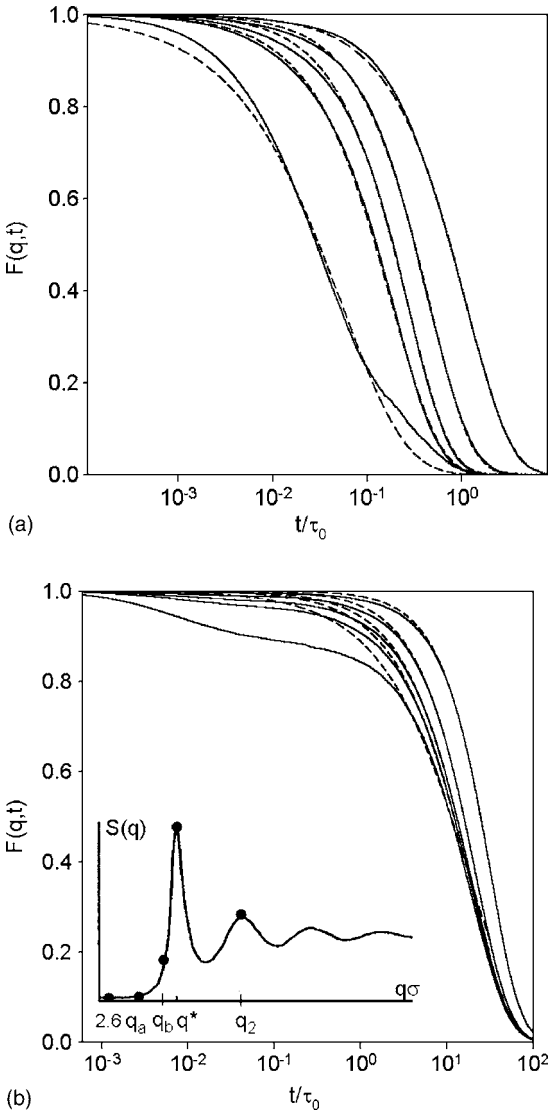

FIG. 3. Incoherent dynamic structure factor (solid lines) with stretched exponential fits (dashed lines). (a) $\phi=0.43$; dimensionless wave vectors from left: $q_2=12.70$, $q^*=6.74$, $q_b=5.36$, $q_a=3.98$, 2.6. (b) $\phi=0.55$; dimensionless wave vectors from left: $q_2=12.97$, $q^*=7.21$, $q_b=5.68$, $q_a=4.14$, 2.6. Inset: schematic of static structure factor with wave vectors for $F(q,t)$ calculations marked.

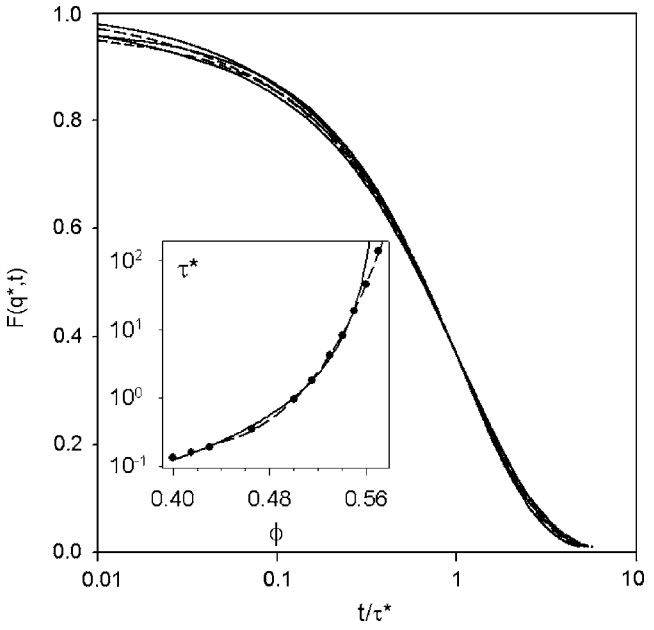

FIG. 4. Incoherent dynamic structure factor at the cage peak as a function of scaled time, $F(q=q^*,t)$ vs $t/\tau(q^*)$, for $\phi=0.43$ (solid), 0.465 (dashed), 0.5 (solid), 0.53 (dashed), 0.55 (solid). Inset: α relaxation time as a function of volume fraction with a critical power law fit, $\tau^* \sim (\phi_c-\phi)^{-\gamma}$ where $\phi_c=0.57$ and $\gamma \sim 2.4$ (solid line), and an exponential in barrier height fit, $\tau^* \sim e^{aF_B}$ with $a \sim 0.95$ (dashed line).

(not shown) a substantial collapse (to within a factor of two) for the barrier controlled slow dynamics regime corresponding to $\phi=0.5-0.57$.

An interesting question is whether for a given wave vector the incoherent dynamic structure factor at various volume fractions can be superimposed onto a master curve. To address this we normalize the time axis by the characteristic wave vector dependent relaxation time, $\tau(q,\phi)$. Results for the cage-scale structure factor $F(q^*,t/\tau^*)$ are shown in Fig. 4. An excellent collapse is obtained suggesting structural relaxation is controlled by a single characteristic time both at lower fluid-like volume fractions (no barrier) and at high (barrier hopping controlled) volume fractions. Detailed analysis of calculations for the other four wave vectors has been performed which we only briefly summarize. The highest wave vector $F(q_2,t)$ results do not collapse well, likely because the short time dynamical process can induce significant relaxation on this smallest length scale. However, if time is nondimensionalized by the relaxation time when $F(q_2,t)=0.1$, then the final stages of the decay (last ~30%) collapse well when barriers are greater than the thermal energy ($\phi \geqslant 0.5$). A good collapse of $F(q,t/\tau(q,\phi))$ is found for the smallest wave vector ($q\sigma=2.6$) when $\phi>0.5$, and a very good or excellent collapse is found at all volume fractions for q_a and q_b.

TABLE I. Effective exponents extracted from fitting the volume fraction dependence of the characteristic decay time of the incoherent structure factor at five wave vectors to an ideal MCT critical power law form, $\tau(q) \propto (\phi_c-\phi)^{-\gamma(q)}$. All fits are performed over the range $\phi=0.5-0.55$.

	$\gamma(\phi_c=0.57)$	$\gamma(\phi_c=0.58)$
$\tau(q\sigma=2.6)$	1.88	2.40
$\tau(q=q_a)$	2.10	2.68
$\tau(q=q_b)$	2.27	2.89
$\tau(q=q^*)$	2.38	3.04
$\tau(q=q_2)$	2.59	3.31

The shape of the dynamic structure factor at intermediate times can be fit by

$$F(q,t) \sim \exp\{-[t/a\tau(q)]^{\beta}\}, \tag{7}$$

where the exponent β quantifies nonexponentiality. Examples are shown in Fig. 3. The fit parameter $a \sim 1$ is weakly ϕ dependent. Effective exponents have been extracted for the intermediate three wave vectors studied by fitting over the range $0.1<F(q,t)<0.8$. The exponents are close to unity and very weakly dependent on volume fraction with: $\beta(q_a) \cong 1.06 \pm 0.06$ and $\beta(q_b) \cong 0.98 \pm 0.03$, $\beta(q^*) \cong 0.87 \pm 0.03$ [39].

The root mean square displacement at the α relaxation time, r_*, is shown in Fig. 2. It is ~0.4 and essentially constant below the (naive) mode-coupling transition. For high barrier-dominated volume fractions, r_* increases linearly with ϕ and approaches a particle diameter for the most concentrated system studied. The significantly increased displacement required to achieve structural relaxation at high volume fractions is another indication of decoupling between translation diffusion and structural relaxation [26].

B. Wave vector-dependent decoupling and dynamic correlation length

If single particle dynamics are purely Gaussian then the wave vector dependent relaxation time obeys the Fickian relation $Dq^2\tau(q)=1$. To quantify deviations from Fickian behavior a wave vector-dependent decoupling factor is defined

$$R(q) \equiv Dq^2\tau(q). \tag{8}$$

In the limit $q \to 0$, or if the dynamics are smooth (e.g., below ϕ_{MCT} in our approach), Gaussian behavior must or is expected to occur, respectively, corresponding to $R(q) \to 1$. Calculations of $R(q)$ at several volume fractions are shown in Fig. 5. For volume fractions below the emergence of a barrier $R(q) \sim 1$ and q independent, i.e., diffusive type motion. For $\phi>0.43$, $R(q)$ is an increasing function of wave vector and volume fraction. MCT predicts (for $\phi<\phi_{MCT}$) $R(q) \sim 1$ for $q\sigma \leqslant 5$ [40], consistent with our results below the (naive) ideal glass transition volume fraction. Our non-MCT finding of $R(q)>1$ for $\phi>\phi_{MCT}$ is a manifestation of the crossover to an activated hopping transport mechanism as found in a recent simulation [40,41].

For barrier-controlled dynamics ($\phi \geqslant 0.5$) Fig. 5 shows that the q-dependent decoupling factor is well fit by a parabolic dependence on wave vector

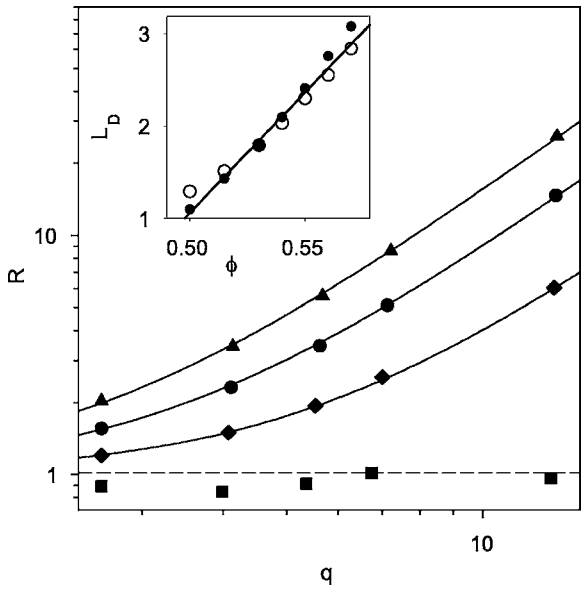

FIG. 5. Wave vector-dependent decoupling factor $R(q)$ for $\phi=0.43$ (squares), 0.50 (diamonds), 0.53 (circles), 0.55 (triangles). Dashed line is $R(q)=1$. Solid curves are fits to the functional form: $Dq^2\tau(q)=1+(L_Dq/2\pi)^2$. Inset: dynamic length scale L_D extracted from the fit of Eq. (9) to the theoretical calculations (filled circles). Open circles are $a(D\tau^*)^{1/2}$, with a prefactor $a=5.65$ adjusted to fit L_D at $\phi=0.53$. Line is a linear fit: $L_D=26\phi-12$.

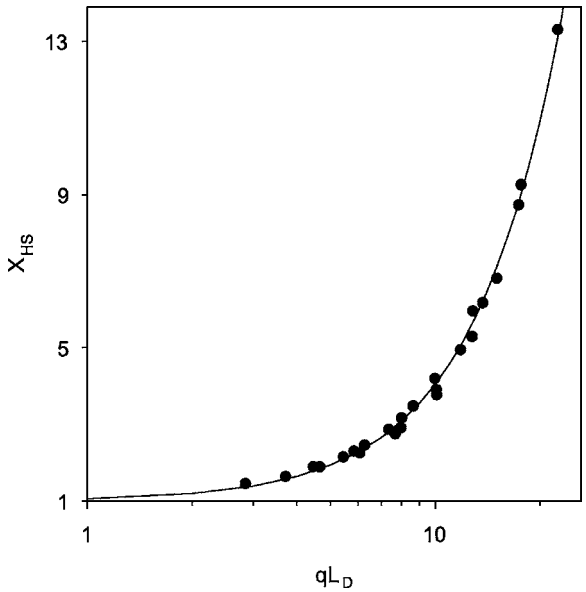

FIG. 6. Alternate wave vector-dependent decoupling factor $X_{HS}=D(\phi)\tau(q;\phi)/(D(0.4)\tau(q;0.4))$ as a function of wave vector nondimensionalized by the dynamic length scale L_D. Points: $\phi=0.5-0.57$ using L_D extracted from Fig. 5. Curve: $1+c(qL_D)^\beta$, with fit exponent $\beta=1.7$.

$$R(q)=1+\left(L_D\frac{q}{2\pi}\right)^2. \tag{9}$$

This functional form is motivated by our analytic statistical dynamical analysis of the crossover from non-Fickian to Fickian diffusion which finds in the Markov limit, corresponding to $F(q,t)\to e^{-t/\tau_D(q)}$, the relaxation rate is given by $\tau_D^{-1}(q)=q^2D/[1+(q\xi_D)^2]$ where the Fickian crossover or viscoelastic length obeys $\xi_D\propto\sqrt{D\tau^*}$ [38]. The latter result has also been obtained based on a coarse grained kinetically constrained or dynamic facilitation model [42]. The length scale L_D extracted by using Eq. (9) is plotted as a function of volume fraction in the inset to Fig. 5. It varies from one to three particle diameters and increases roughly linearly with volume fraction. The unfilled circles in the inset of Fig. 5 are proportional to our calculations of $\sqrt{D\tau^*}$, which clearly follow a very similar ϕ dependence thereby demonstrating $L_D\propto\sqrt{D\tau^*}$ to high accuracy.

Recent BLJM simulations [43] have quantified non-Gaussian relaxation via a wave vector-dependent decoupling factor determined from the incoherent dynamic structure factor

$$X=\frac{\tau(q,T)D(T)}{\tau(q,T_0)D(T_0)}, \tag{10}$$

where T_0 is the onset temperature [8] for slow dynamics. Wave vectors were normalized by a temperature dependent coherence length $\ell(T)$ extracted from the wave vector dependence of a particular multipoint collective dynamic structure factor. This decoupling factor at various temperatures was then found to collapse (for $0.6<q\sigma<7.21$) onto a single curve which is well fit by: $X[q\ell(T)]\sim 1+[q\ell(T)/10]^\beta$ with $\beta\sim 1.6$. To make contact with this study we define the analogous decoupling factor appropriate for our athermal hard-sphere system

$$X_{HS}=\frac{\tau(q,\phi)D(\phi)}{\tau(q,\phi=0.4)D(\phi=0.4)}. \tag{11}$$

The lowest volume fraction for which we have performed calculations, $\phi=0.4$, is employed as an effective onset point used only for (q dependent) normalization. The normalized quantity $X_{HS}(qL_D)$ for $2.6<q\sigma<7.3$ and $\phi\geq 0.5$ is shown in Fig. 6 (for $\phi<0.5$ there is no significant decoupling). Remarkably, our calculations collapse onto a single curve based on the length scale L_D which, although not rigorously equivalent to $\ell(T)$, embodies similar physical ideas. It is significant to note that this collapse is associated with volume fractions where barrier hopping controls the long time relaxation and diffusion. Moreover, it emerges as a consequence of the most elementary aspect of slow glassy dynamics: the initial activated escape from a caged or transiently localized state. Figure 6 shows that an adjusted power law of the form found in the simulation study [43], $X_{HS}(qL_D)\sim 1+c(qL_D)^\beta$, is an excellent description of our master curve for $\beta=1.5-2.0$, with $\beta=1.7$ yielding the most accurate fit.

IV. TIME-DEPENDENT NON-GAUSSIAN PARAMETERS

A. Classic and alternate non-Gaussian parameter

The leading order correction to the Fickian form of the incoherent dynamic structure factor is quantified by the classic non-Gaussian parameter (NGP)

$$\alpha_2(t) = \frac{3}{5}\frac{\langle r^4(t)\rangle}{\langle r^2(t)\rangle^2} - 1. \quad (12)$$

This NGP emphasizes deviations from simple diffusive motion at relatively *short times and small displacements*. In the normal fluid regime its maximum amplitude is typically ~0.1–0.2 [44]. Ideal MCT predicts very small NGP's for *all* fluid states with a maximum value of ~1/3 for hard spheres as the ideal nonergodicity transition is approached [3,40]. In strong contrast, confocal microscopy experiments [45,46] and simulations of polydisperse hard spheres [36,47] find the NGP grows monotonically with volume fraction attaining *much larger* maxima, e.g., ~2–5 at $\phi \sim 0.53$–0.55. Recent molecular dynamics simulations of the BLJM model find the NGP maximum is ~6–10 at a temperature 10% below the empirical MCT critical temperature [48]. Such strongly non-Gaussian behavior has been established in detail by Flenner and Szamel via Brownian dynamics simulations of the BLJM model, and quantitative comparisons with MCT were carried out [27,40,49]. Near the empirically determined critical temperature, MCT severely underestimates the amplitude of the NGP by at least an order of magnitude. Moreover, MCT predicts the NGP saturates as T_c is approached, in qualitative contrast to the monotonic and unbounded growth with cooling found in the simulations. Other fluctuation effects (e.g., bimodal displacement distributions indicating mobility bifurcation) were also found, and all strong non-Gaussian effects were either very poorly accounted for, or absent, in ideal MCT.

Our calculations of the NGP are shown in Fig. 7 [50]. Interestingly, the MCT result that the peak does not exceed ~0.33 is in remarkably good agreement with our results for volume fractions *below* ϕ_{MCT} [Fig. 7(a)]. However, at high ϕ [Fig. 7(b)] the peak greatly exceeds the MCT upper bound and grows strongly in a manner consistent with confocal experiments [45,46] and simulations of polydisperse hard-spheres [36,47] and the binary LJ mixture [27,40,48,49].

An alternate quantification of non-Gaussian behavior has been introduced in recent simulation work of Szamel and Flenner [27]

$$\gamma(t) = \frac{1}{3}\langle r(t)^2\rangle\left\langle \frac{1}{r(t)^2}\right\rangle - 1. \quad (13)$$

In contrast to the classic NGP, this function emphasizes deviations from Fickian behavior at relatively *long times and large displacements*. The simulation study of the BLJM found that the time associated with the maximum of the alternate NGP closely tracks the α relaxation time (a factor of ~1.5–2 times larger but with the same temperature dependence), in qualitative contrast with the classic NGP. Our calculations of the alternate NGP are shown in Fig. 8. Its shape, and time and amplitude of the maximum, are all clearly different from the behavior of the classic NGP, in a manner qualitatively very similar to that found in simulation [27].

B. Characteristics of the maximum non-Gaussian state

The maximum value of the classic NGP, $\alpha_{2,\max}$, is shown as a function of volume fraction in Fig. 9. The peak height of

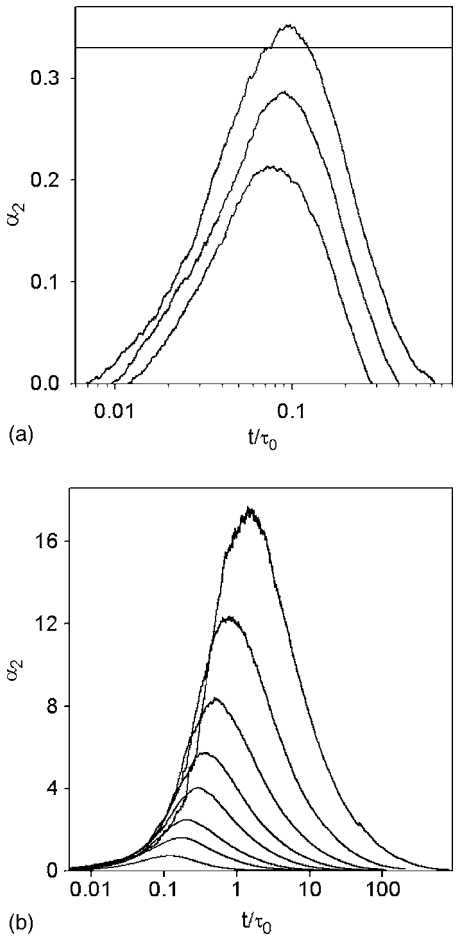

FIG. 7. Classic non-Gaussian parameter as a function of reduced time. (a) Low volume fractions: ϕ=0.4, 0.415, 0.43; horizontal line indicates the ideal MCT limiting maximum value $\alpha_{2,\max} \sim 0.33$. (b) High volume fractions: ϕ=0.465, 0.5, 0.515, 0.53, 0.54, 0.55, 0.56, 0.57.

the alternate NGP is shown in the inset of Fig. 10, and to a remarkably good approximation is proportional to the amplitude of the classic NGP, obeying $\gamma_{\max} \sim 8.8\ \alpha_{2,\max} - 2.7$. This suggests a deep connection between non-Fickian dynamics on relatively short time/distance scales (early aspects of cage escape) and the final α relaxation process (barrier hopping). Such a connection between relatively short and long time cage escape dynamics has been repeatedly found in experimental studies of thermal glass forming materials [1]. The alternate NGP maximum is significantly larger than its classic analog. This seems intuitive since the α process is associated with rare fluctuations needed to surmount the barrier, a process likely more heterogeneous than the in-cage process (late β stage) that the classic NGP probes. Recent simulations of the BLJM model also find a linear relationship between the peak amplitudes of the NGP and its alternate analog [27,51]. Near T_c the alternate NGP amplitude is ~3.5 and 11 for the two mixture species, which is larger than the classic NGP, although smaller than our monodisperse hard-sphere fluid results.

Figure 9 shows the volume fraction dependence of $\alpha_{2,\max}$ can be described as an exponential function of ϕ with a

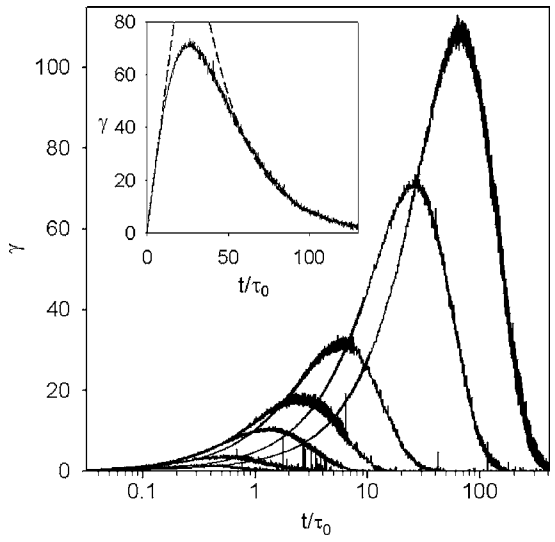

FIG. 8. Alternate non-Gaussian parameter as a function of reduced time for ϕ=0.43, 0.465, 0.5, 0.515, 0.53, 0.55, 0.56. Inset: Alternate NGP for ϕ=0.55 on linear time scale (solid line) with a linear short-time fit, $\gamma \sim 4.7(t/\tau_0)$ and exponential long-time fit $\gamma \sim e^{-0.037(t/\tau_0)}$ (dashed).

change in slope near the volume fraction where the barrier is of order the thermal energy, or alternatively as an empirical critical power law if the barrier is not too high. The latter qualitative behavior is also found in the Brownian BLJM simulations if temperature is not too low [49]. However, the best, simplest and most physically intuitive functional form that describes our theoretical results over the entire volume

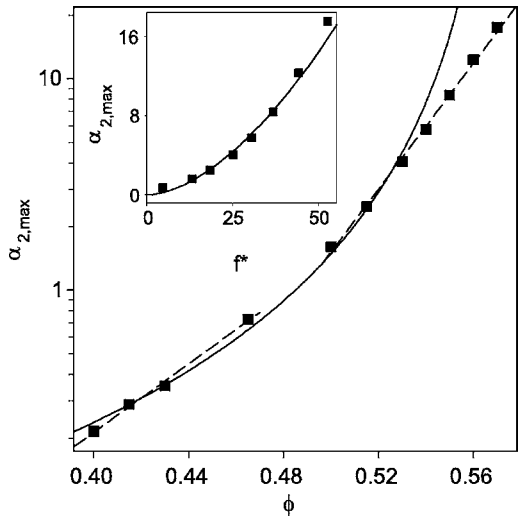

FIG. 9. Maximum value of the NGP as a function of volume fraction (points). Error bars are symbol size or smaller. Solid curve is a critical power law fit for the lower volume fraction regime: $\alpha_{2,\max} \propto (\phi_c - \phi)^{-\nu}$ with ϕ_c=0.575, $\nu \simeq 2.17$; a critical power law also describes the higher volume fraction regime well (not shown) for $0.5 \leqslant \phi \leqslant 0.55$ with a significantly smaller apparent exponent of $\nu \sim 1.5$. Dashed lines are exponential fits: $\alpha_{2,\max} \propto \exp(b\phi)$ with b =18.7 (low ϕ), 34.3 (high ϕ). Inset: maximum of classic non-Gaussian parameter plotted versus the maximum restoring force (f^*). Curve: $\alpha_{2,\max} \propto f^{*1.73}$.

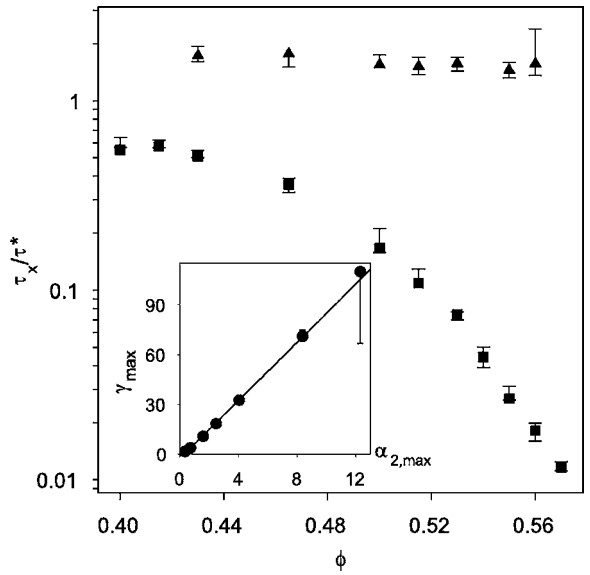

FIG. 10. Time scales of the two non-Gaussian parameters compared to the α relaxation time, with error bars. Squares: τ_α/τ^*. Up triangles: τ_γ/τ^*. Inset: maximum of alternate non-Gaussian parameter, $\gamma_{\max}$, plotted versus the maximum of classic NGP, $\alpha_{2,\max}$. Error bars (vertical and horizontal) are symbol size or smaller except where shown. Linear fit: $\gamma_{\max} \cong 8.8\alpha_{2,\max} - 2.7$.

fraction regime is a power law in the maximum cage restoring force, $\alpha_{2,\max} \propto f^{*1.73} \propto e^{31\phi}$ (inset to Fig. 9). This seems natural since the degree of nondiffusive behavior is expected to be maximized when the effective caging force on a particle is largest. Recall the location of the maximum restoring force at R^* is a small length scale (see Fig. 2) corresponding to the early stages of cage escape [52].

It is of interest to ask how far a particle has typically diffused (i.e., the root mean square displacement) when the classic NGP achieves its maximum, r_α; results are shown in Fig. 2. Below the naive MCT crossover $r_\alpha \sim 0.3$ and is constant, while above $\phi_{\rm MCT}$ we find r_α diminishes with increasing volume fraction. At high volume fractions $r_\alpha \lesssim 0.1$ and lies just beyond the location of maximum restoring force (R^*) and well below the barrier. The root mean square displacement associated with the peak alternate NGP is also shown in Fig. 2. In the Brownian BLJM simulations this quantity is approximately half a particle diameter at high temperature, and then monotonically increases below the onset temperature growing to ~0.9–1.2 particle diameters at the lowest temperature examined [27]. As found in this simulation, our crossover length is constant and of order $\sigma/2$ prior to the MCT crossover, and then increases (by a factor of ~2) with volume fraction. This length scale varies nearly in parallel with the α relaxation displacement r_* at high volume fractions.

The time associated with the maximum of the classic NGP, τ_α, is remarkably slowly varying and at high volume fractions increasingly lags other characteristic time scales. Figure 10 shows the ratio of the NGP peak and α times (τ_α/τ^*) decreases from $\gtrsim$0.5 below the naive MCT crossover, to ~0.15 at ϕ=0.5, to less than 0.01 at very high ϕ. Hence, as volume fraction increases the α time occurs in-

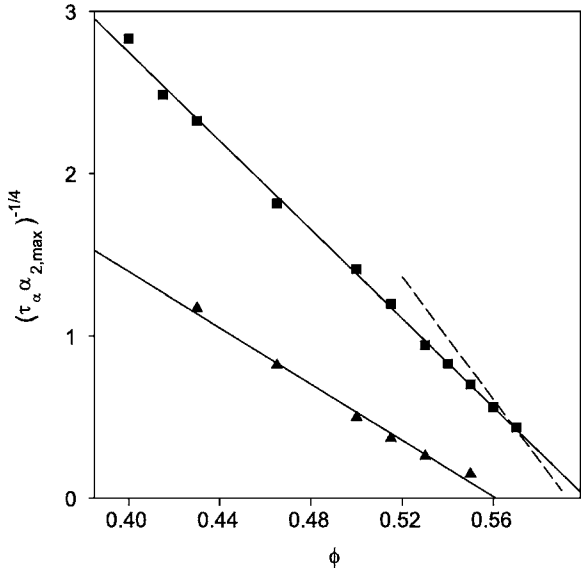

FIG. 11. Plot of the theoretical $Q(\phi) \equiv [\tau_\alpha \alpha_{2,\max}]^{-1/4}$ as a function of volume fraction (squares) with a linear fit given by $-13.7\phi+8.2$. The dashed curve is a (excellent) linear fit to the simulation data [36] given by $-18.8\phi+11.1$. Also shown is the theoretical result for the alternate NGP: $[\tau_\gamma \gamma_{\max}]^{-1/4}$ (up triangles) with a linear fit given by $-8.7\phi+4.9$.

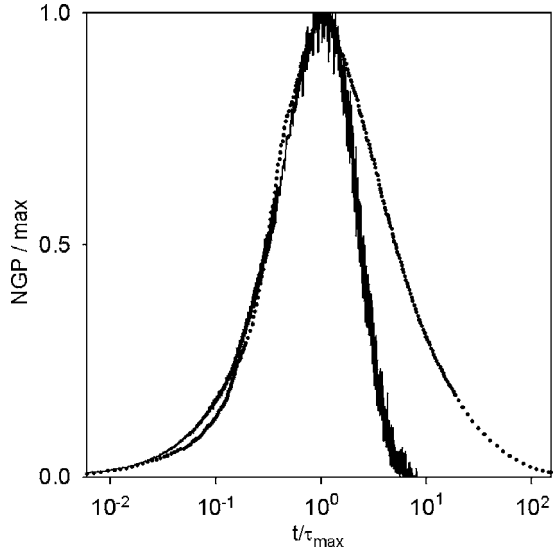

FIG. 12. Classic (dotted line) and alternate (solid line) non-Gaussian parameters for $\phi=0.55$, normalized by their maximum values, as a function of normalized time.

creasingly farther into the long-time branch of the NGP, consistent with simulations [27,40]. The value of the NGP at the α time relative to its maximum is a (approximately linearly) decreasing function of volume fraction. This indicates that deep in the glassy regime the classic NGP is not a measure of structural relaxation [27]. By contrast, the time associated with the maximum *alternate* NGP, τ_γ, closely tracks the α time, as demonstrated in Fig. 10. Consistent with simulation [27], τ_γ/τ^* is slightly greater than unity and roughly constant with volume fraction.

Odagaki and Hiwatari [53] have argued the product $\tau_\alpha \alpha_2(\tau_\alpha)$ is sensitive to the non-Gaussian aspects of particle motion. In particular, the quantity $Q=[\tau_\alpha \alpha_2(\tau_\alpha)]^{-1/4}$ is suggested to decrease roughly linearly with cooling or increase of density. This idea has been recently tested by simulations of a polydisperse hard-sphere fluid [36] for $0.52<\phi<0.59$. A linear dependence of $[\tau_\alpha \alpha_2(\tau_\alpha)]^{-1/4}$ on ϕ was found and an accurate fit to the simulation results is shown in Fig. 11. Note the smooth change of this quantity with volume fraction indicating no qualitative change in the non-Gaussian nature of particle motion and no indication of a singularity. The volume fraction range studied in the simulation corresponds to values at which our theory predicts motion is controlled by activated processes. The theoretical results for $Q(\phi)$ are shown in Fig. 11, and a linear decrease with ϕ is predicted in good agreement with simulation [36]. Moreover, both the theoretical and simulation results extrapolate to a hypothetical ideal glass state ($Q=0$) at a similar volume fraction of $\sim 0.60-0.61$, which is higher than the typically extracted empirical value for self-diffusion ($\sim 0.57-0.58$). Figure 11 also includes theoretical results for the alternate NGP analog of Q. The linear form is remarkably similar to its classic analog except for the overall magnitude, again indicating a strong connection between the early and final stages of cage escape.

C. Form of the time dependence of the non-Gaussian parameter

The temporal form of the classic and alternate non-Gaussian parameters show similar volume fraction dependences. At low volume fractions (below the naive MCT transition), the doubly normalized NGP's, $\alpha_2(t/\tau_\alpha)/\alpha_{2,\max}$ and $\gamma(t/\tau_\gamma)/\gamma_{\max}$, superpose well (not shown) and the short- and long-time branches are nearly symmetric. At high volume fractions, the long time branch of the NGP monotonically broadens with increasing ϕ. This trend is consistent with simulation and experiment [40,47,49], although the breadth of the theoretical function is considerably smaller [54]. The breadth of the alternate NGP weakly increases with volume fraction primarily due to its short time tail (which also broadens slightly in the classic NGP).

A representative comparison of the shapes of the classic and alternate NGP's in the high volume fraction regime is shown in Fig. 12. The inset of Fig. 8 demonstrates the short-time branch of the alternate NGP is a linear function of time, while the long-time branch decays exponentially with a characteristic time of $(1.5-2)\tau^*$. This sharp long-time cutoff contrasts with the more symmetric form of the classic NGP, and is consistent with the idea [27] that the alternate NGP captures dynamical fluctuation effects associated with structural relaxation.

V. TRAJECTORY DISPLACEMENTS AND MOBILITY BIFURCATION

A. Evolution of displacement distributions

The real space analog of $F(q,t)$, the van Hove function, quantifies the probability density a particle has moved a dis-

tance r in a time t. We follow previous simulation studies [27,40,47] and define a displacement probability distribution as the logarithim (base 10) of the single particle displacements. This quantity has been computed at several characteristic times: the α relaxation time, the Kramers time, times at which the root mean square displacement (MSD) corresponds to notable features of the nonequilibrium free energy profile (localization length r_L, maximum restoring force location R^*, barrier location r_B, reaction point $r^\dagger$), and times when the root MSD equals one, two, and three particle diameters. Typical results are presented in Fig. 13. At low volume fractions (no barrier) Fig. 13(a) shows the displacement distribution has a unimodal shape. It is Gaussian at short times, broadens to a non-Gaussian shape at intermediate times, and recovers a Gaussian form at long times.

At high volume fractions the intermediate-time distribution becomes bimodal. The two peak bifurcation is well delineated for $\phi \geqslant 0.5$ (corresponding to barriers $> k_B T$), and persists for a substantial period. For $\phi=0.55$ [Fig. 13(b)] the distribution is bimodal for roughly $0.16 \leqslant \langle r^2 \rangle^{1/2} \leqslant 1$. At the onset of bimodality the displacement between the fast and slow peaks is roughly one half a particle diameter [55]. Such very strong bimodality is consistent with recent simulations [47] of a polydisperse repulsive force fluid at $\phi=0.55$. The bimodality is most prominent at a time of order the α relaxation time, and is essentially nonexistent at times when the classic NGP parameter peaks. This is consistent with recent BLJM simulations [27,40] which have established the classic NGP does not accurately identify the time scale on which dynamic heterogeneity and activated hopping is maximized. The slow and fast peak locations evolve differently, with fast peak growth and motion accounting for long-time escape. At short times, the slow peak occurs roughly at $\langle r^2(t) \rangle$, but quickly saturates near the dynamic plateau length scale $\langle r^2 \rangle^{1/2}_{\text{plateau}}$ (the displacement of most anomalous diffusion [26] as shown in Fig. 2). The diminishment of the slow peak, which begins before the saturation of its location, culminates in its disappearance when $\langle r^2 \rangle^{1/2}=1-2$. The emergence of the fast peak coincides well with saturation of the slow displacement. When the slow peak is significant in amplitude, the fast peak moves only very slowly from its initial location, which is beyond the barrier and closely coupled to the reaction point. At long times ($t > \tau^*$) the slow peak location increases as $t^{1/2}$.

The α relaxation time is a judicious characteristic time for studying the bimodality since our results (as well as simulations [27]) indicate the bifurcation of trajectories near τ^* (or the time the alternate NGP peaks) is particularly strong. Displacement distributions at the α time for several volume fractions (Fig. 14) show that the distribution broadens with increasing volume fraction below the naive MCT transition, and above ϕ_{MCT} separates into two peaks of comparable intensities. The fast peak encompasses approximately sixty percent of the trajectories at this time. The inset of Fig. 14 shows that the most probable displacement of the fast particle population at the α time, $r_{\text{fast}}(\tau^*)$, grows with volume fraction, a trend directly correlated with the growing decoupling of the diffusion constant and α time with increasing ϕ [26,27].

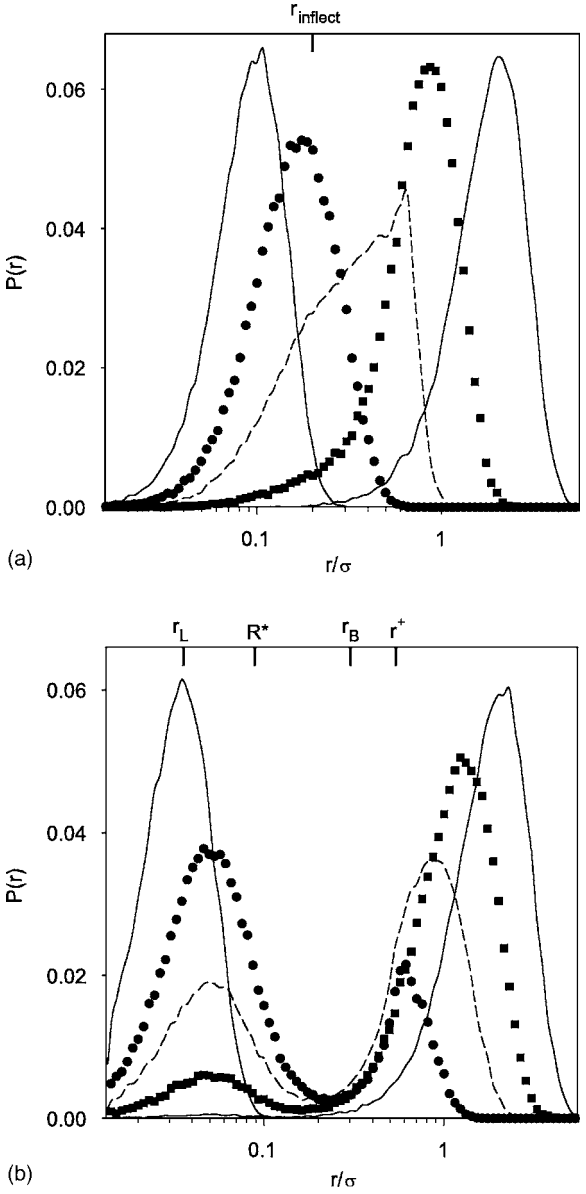

FIG. 13. Displacement distribution at key times and values of the root MSD. (a) $\phi=0.43$, from left: $\langle r^2(t) \rangle^{1/2}=0.1$ (left solid curve), $\langle r^2(t) \rangle^{1/2}=0.19$ (inflection point, circles), $t=\tau^*$ (dashed curve), $t=\tau_K$ (squares), $\langle r^2(t) \rangle^{1/2}=2$ (right solid curve). Vertical marks on the upper axis corresponds to the position of the inflection point of $F_{\text{eff}}(r)$. (b) $\phi=0.55$. Solid and dashed lines, from left: $\langle r^2(t) \rangle^{1/2}=r_L$ (left solid curve), $\langle r^2(t) \rangle^{1/2}=r_B$ (circles), $t=\tau^*$ (dashed curve), $t=\tau_K$ (squares), $\langle r^2(t) \rangle^{1/2}=2$ (right solid curve). Vertical marks on the upper axis correspond to the positions of the local minimum, maximum restoring force, barrier, and reaction point of the effective free energy.

B. Recovery of a Gaussian distribution

A recent Brownian simulation study of the BLJM model [56] quantified the onset time for Fickian diffusion as when the displacement distribution peak reaches 90% of the value corresponding to a purely Gaussian distribution. The root MSD required to achieve such Gaussian behavior was reported to increase from slightly less than a particle diameter

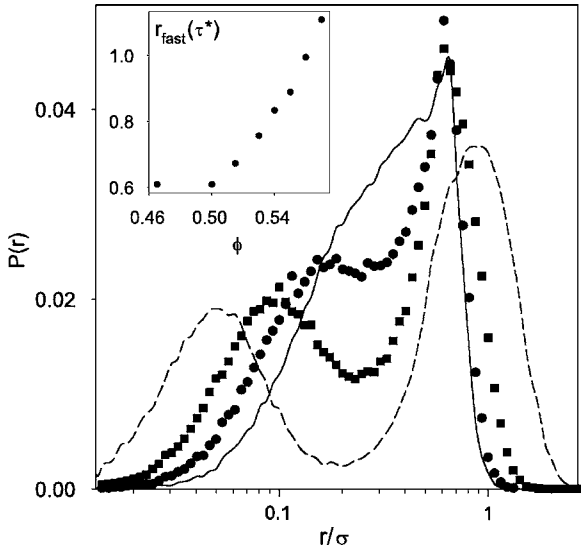

FIG. 14. Displacement distributions at the α relaxation time for $\phi=0.43$ (solid curve), 0.465 (circles), 0.5 (squares), 0.55 (dashed curve). Inset is the most probable displacement of the fast particle population at $t=\tau^*$.

at high temperatures to ~2.7 particle diameters at the empirically deduced T_c. We have compared our displacement distribution results to a Gaussian function with the same MSD. Since our data set is limited we cannot make precise statements about when Fickian behavior is recovered. However, at a general level we can state that for $\phi<0.5$ the displacement distribution when $\langle r^2\rangle^{1/2}=1$ is Gaussian according to the 90% criterion, but for $\phi>0.5$ it is not. At a qualitative level this is consistent with simulations [56]. Results for the high barrier $\phi=0.55$ system are shown in Fig. 15. When $\langle r^2\rangle^{1/2}=1$ the distribution still has a significant slow peak (not shown), and therefore the fast (higher) peak is substantially smaller than the corresponding Gaussian curve. At $\langle r^2\rangle^{1/2}=2(3)$ the slow peak has disappeared and the (fast) peak height is about 93(99)% of the Gaussian value. From Fig. 2 the root MSD at the α time is ~0.7, significantly smaller than the Fickian onset displacement which is reached at times well in excess of the α relaxation time. All these theoretical results are consistent with the binary LJ mixture simulations [56].

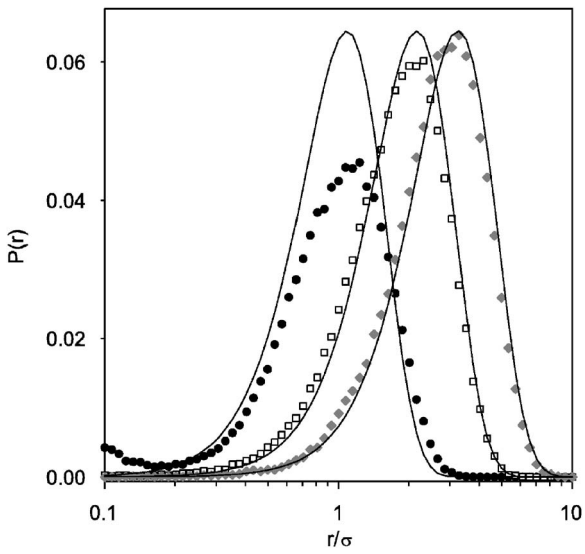

FIG. 15. Displacement distributions for $\phi=0.55$ at times corresponding to $\langle r^2\rangle^{1/2}=1$ (filled circles), 2 (open squares), and 3 (shaded diamonds) particle diameters. Curves are Gaussian distributions with corresponding mean square displacements and consistent units.

VI. SUMMARY AND CONCLUSIONS

We have employed Brownian stochastic trajectory methods [26] to study non-Gaussian fluctuation effects in glassy hard-sphere fluids based on a nonlinear Langevin equation theory of *single particle* motion [9,29]. The incoherent dynamic structure factor on the cage scale exhibits a nearly constant, modest degree of stretching, with the relaxation curves for many volume fractions superimposing when time is normalized by the α relaxation time. The α time increases exponentially with entropic barrier height, or as a MCT-like critical power law in the volume fraction until barriers exceed $\sim 5k_BT$. The deviation of the incoherent dynamic structure factor from a Gaussian form increases markedly with volume fraction as demonstrated by the rapidly growing amplitude of the classic NGP which is well described by a power law in the maximum restoring force of the nonequilibrium free energy profile. At the naïve MCT volume fraction the NGP peak is ~1/3, in remarkable (and surprising) accord with *full* ideal MCT calculations [3,40]. However, with increasing volume fraction and the emergence of significant entropic barriers the NGP maximum grows very strongly reaching a value of ~12 for $\phi=0.56$. The time associated with the NGP peak is comparable with the α relaxation time at low volume fractions, but becomes much smaller than the α time when barriers are significant. The shift of the corresponding MSD to smaller displacements with volume fraction is strong, and the relevant length scale approaches the displacement of maximum cage restoring force, R^*.

An alternate non-Gaussian parameter [27], $\gamma(t)$, was also computed and is of a different shape than $\alpha_2(t)$. However, its peak magnitude is proportional to that of the classic analog, suggesting a deep connection between this measure of non-Fickian motion on intermediate (late β process) and long (α process) length scales. The time associated with the alternate NGP peak is very nearly the α relaxation time for all volume fractions, and long time exponential decay is found. However, the corresponding root MSD increases monotonically with volume fraction from ~0.4 to ~1, consistent with the increase of the MSD at the α relaxation time.

Space-time decoupling has been quantified via the quantity $R(q)=q^2D\tau(q)$. Below the naive MCT transition the $R(q)\sim 1$ Gaussian result is found in accord with full MCT calculations [40]. However, at higher volume fractions $R(q)$ becomes increasingly wave vector dependent and $F(q,t)$ is strongly nondiffusive. These changes reflect decoupling of translational motion and relaxation [26], which our *model-independent* analytic analysis [38] suggests is a consequence

of strong coupling of particle mass transport and (single particle) stress relaxation on finite length scales. Remarkable agreement of the shape and scaling properties of the theoretical $R(q)$, and the Fickian crossover length scale, with a recent simulation study of the binary LJ mixture [43] is found. The particle displacement required for recovery of the diffusive form of $F(q,t)$ increases by a factor of three as volume fraction (barrier) grows from 0.5 to 0.57 ($\sim 1-6.7\ k_BT$).

Displacement distributions exhibit non-Gaussian behavior at intermediate times, evolving into a bimodal form with slow and fast subpopulations at high volume fractions associated with a broad distribution of hopping rates. This behavior is directly correlated with the growth of the decoupling factor $D\tau^*$ (fractional Stokes-Einstein relation) [26] and a nondiffusive wave vector dependence of the α time [26,38]. The root MSD required to recover a real space Gaussian distribution increases with volume fraction, exceeding a particle diameter as barriers become of significant height.

Our primary goal has been to investigate how much of the strongly non-Gaussian fluctuation phenomena associated with glassy dynamics as manifest in two point dynamic correlations can be understood from the elementary events of transient localization, early stages of cage escape, and activated hopping of *single* particles on the cage length scale. We believe our results are relevant to slow dynamics in dense hard-sphere fluids, simple thermal liquids, and athermal colloidal suspensions. However, the presence of hydrodynamic interactions (HI), residual charge and particle size polydispersity in real suspensions complicates to some extent quantitative confrontation with experiment. Certainly the question of how *many body* hydrodynamic interactions modify activated processes is not well understood. Early arguments [3] and some experiments [56] claimed hopping processes are suppressed in colloidal suspensions due to lack of momentum conservation and/or HI. It is true that ideal MCT critical power laws can be well fit to the diffusion constant and α time of hard-sphere suspensions (up to ~ 0.57) [3,57]. However, there remains the fact that experiments [45,46] and/or Brownian and Newtonian simulations [36,47] on polydisperse hard-sphere-like fluids *do* find *very large* non-Gaussian parameters, significant translation-relaxation decoupling, and non-Gaussian particle distributions including bimodal forms which is not predicted by MCT. Within the context of our approach, and given the recent simulation findings that activated processes emerge above the empirically deduced MCT transition [6–8], a possible resolution of this puzzle is that dynamics in the precursor regime involves activated hopping over relatively low entropic barriers. The consequences of the latter for physical quantities not directly determined by, and/or not very sensitive to, non-Gaussian fluctuation effects might well be accurately described by a self-consistent Gaussian-like theory of density fluctuations such as ideal MCT. Concerning simulations of thermal mixtures (BLJM) and hard-sphere-like fluids, quantitative complications arise since the models generally involve polydispersity, repulsive forces with some degree of softness, and/or weak attractive interactions. Nevertheless, within these caveats our many present and prior [26] predictions for the nature and origin of multiple non-Gaussian fluctuation effects based on a *single* simple (but nonperturbative) microscopic physical picture devoid of fitting parameters appear to be in excellent qualitative, and often semiquantitative, agreement with a variety of experiments and computer simulations. We hope new simulations and experiments are designed and performed to test our theoretical predictions.

ACKNOWLEDGMENTS

The authors acknowledge the extensive contributions of Dr. Vladimir Kobelev to the development of the Brownian simulation method, as well as many insights on the results. Helpful discussions with Professor G. Szamel and Professor S. Kumar are gratefully acknowledged. This work was supported by the U.S. Department of Energy, Division of Materials Sciences under Contract No. DEFG02-91ER45439 through the Frederick Seitz Materials Research Laboratory.

[1] For reviews see: C. A. Angell, K. L. Ngai, G. B. McKenna, P. F. McMillan, and S. W. Martin, J. Appl. Phys. **88**, 3113 (2000); S. Glotzer, J. Non-Cryst. Solids **274**, 342 (2000); M. D. Ediger, Annu. Rev. Phys. Chem. **51**, 99 (2000); R. Richert, J. Phys.: Condens. Matter **14**, R703 (2002).

[2] P. G. Debenedetti and F. H. Stillinger, Nature **410**, 259 (2001).

[3] W. Gotze and L. Sjogren, Rep. Prog. Phys. **55**, 241 (1992); W. Gotze, J. Phys.: Condens. Matter **11**, A1 (1999); M. Fuchs, Transp. Theory Stat. Phys. **24**, 855 (1995).

[4] T. R. Kirkpatrick, D. Thirumalai, and P. G. Wolynes, Phys. Rev. A **40**, 1045 (1989); X. Xia and P. G. Wolynes, Phys. Rev. Lett. **86**, 5526 (2001); X. Xia and P. G. Wolynes, Proc. Natl. Acad. Sci. U.S.A. **97**, 2990 (2000).

[5] J. P. Bouchard, L. Cugliandolo, J. Kuchan, and M. Mezard, Physica A **226**, 243 (1996); J. P. Bouchard and M. Mezard, Prog. Theor. Phys. Suppl. **126**, 181 (1997); L. Angelani, R. Di Leonardo, G. Ruocco, A. Scala, and F. Sciortino, Phys. Rev. Lett. **85**, 5356 (2000).

[6] W. Kob, J. Phys.: Condens. Matter **11**, R85 (1999); W. Kob and H. C. Andersen, Phys. Rev. E **51**, 4626 (1995); W. Kob, *ibid.* **52**, 4134 (1995).

[7] H. Lowen, J. P. Hansen, and J. N. Roux, Phys. Rev. A **44**, 1169 (1991); T. Gleim, W. Kob, and K. Binder, Phys. Rev. Lett. **81**, 4404 (1998); H. Miyagawa, Y. Hitatari, B. Bernu, and J. P. Hansen, J. Chem. Phys. **88**, 3879 (1988).

[8] B. Doliwa and A. Heuer, Phys. Rev. E **67**, 030501(R) (2003); **67**, 031506 (2003); Y. Brumer and D. R. Reichman, *ibid.* **69**, 041202 (2004).

[9] K. S. Schweizer and E. J. Saltzman, J. Chem. Phys. **119**, 1181 (2003).

[10] E. J. Saltzman and K. S. Schweizer, J. Chem. Phys. **119**, 1197 (2003).

[11] Y.-L. Chen and K. S. Schweizer, J. Chem. Phys. **120**, 7212 (2004).

[12] Y. L. Chen, V. Kobelev, and K. S. Schweizer, Phys. Rev. E **71**, 041405 (2005).

[13] G. Yatsenko and K. S. Schweizer, J. Chem. Phys. (to be published).

[14] K. S. Schweizer and E. J. Saltzman, J. Chem. Phys. **121**, 1984 (2004); E. J. Saltzman and K. S. Schweizer, *ibid.* **121**, 2001 (2004).

[15] E. J. Saltzman and K. S. Schweizer, J. Phys.-Condensed Matter (to be published).

[16] F. T. Oyerokun and K. S. Schweizer, J. Chem. Phys. **123**, 224901 (2005).

[17] K. Chen and K. S. Schweizer, J. Chem. Phys. (to be published).

[18] V. Kobelev and K. S. Schweizer, J. Chem. Phys. **123**, 164902 (2005); *ibid.* **123** 164903 (2005).

[19] V. Kobelev and K. S. Schweizer, Phys. Rev. E **71**, 021401 (2005).

[20] R. Rao, V. Kobelev, Q. Li, J. A. Lewis, and K. S. Schweizer, Langmuir **22**, 2441 (2006).

[21] W. Kob, C. Donati, S. J. Plimpton, P. H. Poole, and S. C. Glotzer, Phys. Rev. Lett. **79**, 2827 (1997); S. C. Glotzer, V. N. Novikov, and T. B. Schroeder, J. Chem. Phys. **112**, 509 (2000).

[22] R. Yamamoto and A. Onuki, Phys. Rev. E **58**, 3515 (1998).

[23] D. Perera and P. Harrowell, J. Non-Cryst. Solids **235**, 314 (1998).

[24] J. P. Garrahan and D. Chandler, Phys. Rev. Lett. **89**, 035704 (2002).

[25] C. Toninelli, M. Wyart, L. Berthier, G. Biroli, and J. P. Bouchaud, Phys. Rev. E **71**, 041505 (2005).

[26] E. J. Saltzman and K. S. Schweizer, J. Chem. Phys. **125**, 044509 (2006).

[27] E. Flenner and G. Szamel, Phys. Rev. E **72**, 011205 (2005).

[28] T. R. Kirkpatrick and P. G. Wolynes, Phys. Rev. A **35**, 3072 (1987).

[29] K. S. Schweizer, J. Chem. Phys. **123**, 244501 (2005).

[30] K. Kawasaki, Physica A **208**, 35 (1994); K. Kim and T. Munakata, Phys. Rev. E **68**, 021502 (2003); D. S. Dean, J. Phys. A **29**, L613 (1996); T. Munakata, Phys. Rev. E **67**, 022101 (2003).

[31] A. J. Archer and M. Rauscher, J. Phys. A **37**, 9325 (2004); D. Reguera and H. Reiss, J. Chem. Phys. **120**, 2558 (2004); R. Evans, Adv. Phys. **28**, 143 (1979); M. B. Marconi and P. Tarazona, J. Chem. Phys. **110**, 8032 (1999).

[32] J. P. Hansen and I. R. McDonald, *Theory of Simple Liquids* (Academic Press, London, 1986).

[33] H. A. Kramers, Physica (Utrecht) **7**, 284 (1940).

[34] P. Hanggi, P. Talkner, and M. Borkovec, Rev. Mod. Phys. **62**, 251 (1990).

[35] C. Kaur and S. P. Das, Phys. Rev. Lett. **86**, 2062 (2001).

[36] S. K. Kumar, G. Szamel, and J. F. Douglas, J. Chem. Phys. **124**, 214501 (2006).

[37] As discussed in detail previously [26], the choice of reaction point affects the structural decay only very slightly. Smaller values of the reaction point lead to slightly more rapid decay at the larger wave vectors (q_2 and q^*) and indistinguishable decay at the smaller wave vectors. The characteristic decay times for high wave vectors are modestly altered, but the form of their volume fraction dependence is preserved.

[38] K. S. Schweizer and E. J. Saltzman, J. Phys. Chem. B **108**, 19729 (2004).

[39] As discussed in [26], a (presumably unphysical) intermediate superdiffusive regime of the mean square displacement is characteristic of our theory due to the abrupt switching from dynamics on the nonequilibrium free energy profile to Cartesian diffusion. This superdiffusivity is likely the origin of the slightly compressed exponential behavior found at the wave vector q_a.

[40] E. Flenner and G. Szamel, Phys. Rev. E **72**, 031508 (2005).

[41] Although we probe wave vectors up to $q\sigma \sim 12-13$, the high wave vector decrease in $R(q)$ seen at *all* temperatures in recent Brownian simulations [40] is not found in our calculations. We expect our theory recovers this result at sufficiently large wave vectors but its onset is sensitive to our very small length and time scale approximations which are not relevant to the glassy dynamics aspect of the problem.

[42] L. Berthier, D. Chandler, and J. P. Garrahan, Europhys. Lett. **69**, 320 (2005).

[43] L. Berthier, Phys. Rev. E **69**, 020201(R) (2004).

[44] A. Rahman, Phys. Rev. **136**, A405 (1964).

[45] E. R. Weeks and D. A. Weitz, Phys. Rev. Lett. **89**, 095704 (2002); Chem. Phys. **284**, 361 (2002).

[46] W. K. Kegel and A. van Blaaderen, Science **287**, 290 (2000).

[47] D. R. Reichman, E. Rabani, and P. L. Geissler, J. Phys. Chem. B **109**, 14654 (2005).

[48] H. R. Schober, Phys. Chem. Chem. Phys. **6**, 3654 (2004).

[49] G. Szamel and E. Flenner, Europhys. Lett. **67**, 779 (2004).

[50] Our calculations of the classic and alternate non-Gaussian parameters show a weakly negative tail at very short times due to the deterministic small displacement dynamics employed to avoid unphysical excursion into $r<0$ space [26]. The latter does not affect any aspect of the results over the time range of interest presented in the figures.

[51] G. Szamel and E. Flenner (private communication).

[52] Larger reaction displacement choices result in an increase of the influence of activated hopping and therefore an increased $\alpha_{2,\max}$, but this is a moderate effect. For example, for $\phi = 0.53$ over the range of physically sensible choices of the reaction point [26] we find $\alpha_{2,\max}$ changes by 20%. The time corresponding to this peak is, to within the uncertainty of our data, invariant to the choice of reaction point within the physically plausible bounds discussed in Ref. [26].

[53] T. Odagaki and Y. Hiwatari, Phys. Rev. A **43**, 1103 (1991).

[54] The trend that our NGP is narrower than found in simulations and experiments may be due (at least partially) to the fact that such studies involve polydisperse particles or mixtures which we expect will increase the breadth of the distributions of various dynamical processes.

[55] Our implementation of the reaction point does not create this broad separation, but it does affect it quantitatively. The displacement at which the fast peak appears is strongly correlated with the position of the reaction point.

[56] G. Szamel and E. Flenner, Phys. Rev. E **73**, 011504 (2006).

[57] W. van Megen, T. C. Mortensen, S. R. Williams, and J. Muller, Phys. Rev. E **58**, 6073 (1998).